The equal spacing of N points on a sphere with application to partition-of-unity wave diffraction problems

M.J. Peake*, J. Trevelyan, G. Coates

Durham University, School of Engineering and Computing Sciences, Durham, DH1 3LE, United Kingdom

Abstract

This paper addresses applications involving the selection of a set of points on a sphere, in which the uniformity of spacing can be of importance in enhancing the computational performance and/or accuracy of some simulation. For the authors, the motivation for this work arises from the need to specify wave directions in a partition-of-unity approach for numerical analysis of wave diffraction problems. A new spacing method is presented, based on a physical analogy in which an arbitrary number of charged particles are held in static equilibrium on a spherical surface. The new method, referred to in this paper as the Coulomb force method, offers an improvement over simpler methods, e.g., latitude/longitude and discretised cube methods, in terms of both the uniformity of spacing and the arbitrary nature of the number of points N that can be considered. A simple extension to the algorithm allows points to be biased towards a direction of choice. Numerical results of a wave scattering problem solved with a partition-of-unity boundary element method demonstrate the benefits of the algorithm.

Keywords: uniform distribution, sphere, Helmholtz, acoustics, boundary element method, partition of unity

*Corresponding author

Email address: m.j.peake@durham.ac.uk (M.J. Peake)

1. Introduction

There are numerous applications in science and engineering in which a set of N points is to be spaced as uniformly as possible on a spherical surface. The motivation for the authors of this paper is the definition of a set of plane wave directions to form a basis for a partition-of-unity [1] finite or boundary element analysis of wave diffraction. The choice of such a set of directions, being a set of unit vectors on the unit sphere, presents a directly equivalent problem. Confining this discussion to the various three-dimensional wave diffraction algorithms that exist, an efficient spacing algorithm would be of benefit in the plane-wave methods of Perrey-Debain *et al.* [2], in the discontinuous enrichment method of Massimi *et al.* [3], in the variational theory of complex rays of Kovalevsky *et al.* [4], in the ultra weak variational formulation of Luostari *et al.* [5], as well as other Trefftz methods. It is not the intention of the authors to present in this paper a detailed review of such methods; the interested reader is referred to Bettess [6].

Researchers from a diverse set of fields have studied the problem of finding a uniform set of points on sphere. In Monte Carlo approaches, the desire is to produce a set of points that is statistically uniform; that is, a suitable χ^2 test shows no significant deviation from the uniform distribution. Possibly the simplest method to achieve a statistically uniform distribution of points on the unit-sphere was first devised for the unit-circle by von Neumann [7] and extended by Cook [8] for spheres of three dimensions and higher. A sample $\mathbf{x}$ is taken from the uniform distribution on $[-1, 1]^n$, where n is the number of dimensions being considered. The sample is rejected if its Euclidean norm, $\|\mathbf{x}\|$, is greater than 1 and accepted if $\|\mathbf{x}\| \leq 1$. Sampling continues until the desired number of points is obtained. The points are then normalised so that they are placed on the surface of the sphere. This method is adequate for circles and three-dimensional spheres. However, as n increases, the size of the space $\|\mathbf{x}\| > 1$ becomes much larger than the space $\|\mathbf{x}\| \leq 1$; this means the ratio of rejected to accepted points increases rapidly and most of the computational burden is on generating points that will be discarded.

A similar method, presented by Muller [9], uses sample points taken from the normal distribution. This is possible as the multivariate normal distribution is radially symmetric. Given a suitable normal distribution, this method has a lower ratio of rejected to accepted points compared to taking points from the uniform distibution. A family of methods, using the beta distribution, were developed for higher dimensional spheres [10, 11, 12, 13, 14]. The

relationship between these efficient methods was presented by Harman and Vladimir [15].

In mathematics, the 'uniform spacing' of points ordinarily refers to points that fit the statistical, uniform distribution. Conversely, in the physical sciences, 'uniform spacing' of points refers to making the distance or angle between adjacent points equal by maximising or minimising some criterion. One such example of this is the Thomson Problem: determining the minimum energy configuration of N electrons on the surface of a sphere. This is often associated with the Tammes problem in which N points are arranged on the surface of a sphere so that the minimum distance between them is maximised. Erber and Hockney [16] presented equilibrium configuations of charges on a sphere for $2 \leq N \leq 65$. Glasser and Every [17] extended these calculations to $N \leq 101$. Morris *et al.* [18] developed a genetic algorithm that searches for the steepest-decent in energy; with this algorithm, configurations were extended to $N \leq 200$. Saff and Kuijlaars [19] considered configurations of $N \to \infty$, stating that the general pattern of optimal configuation was the same for all values of N.

In the study of meteorology, spherical grids can be used to model the atmosphere. Kurihara [20] stated that a homogeneous density of grid points on a globe is desirable, presenting a new grid system that was almost homogeneous. Sahr *et al.* [21] later reviewed methods of so-called geodesic discrete global grid systems in which the globe, modelled as an oblate spheroid, is divided in to cells; some of these approaches examined ways of making these cells of equal area. It can be desirable to find uniformly spaced points on other surfaces: in operational research, Rubinstein [22] and Smith [23] considered generating random vectors uniformly on the surface of complex, multidimensional surfaces.

This paper concentrates on presenting a new method of producing equally spaced points on the unit-sphere in three-dimensions. This method is valid for arbitrary N and can be modified to fix one or more points on the sphere; a modification to cluster the points towards one point is also shown. This new method is used in the partition-of-unity enrichment of a boundary element method simulation of an acoustic wave scattered by a sphere; these simulations benefit from the ability to specify the position of one point and choose an arbitrary N.

2. Partition-of-unity boundary element method

The following section gives a brief derivation of the partition-of-unity boundary element method (PU-BEM). For a more thorough introduction to the topic of boundary elements, the authors recommend [24] and [25].

Let $\Omega \subset \mathbb{R}^3$ be an infinite acoustic domain containting a smooth scatterer of boundary $\Gamma := \partial\Omega$. Assuming $\exp(-i\omega t)$ time dependence, the wave equation is reduced to the Helmholtz equation:

$$\Delta\phi(\mathbf{q}) + k^2\phi(\mathbf{q}) = 0, \quad \phi \in \mathbb{C}, \mathbf{q} \in \Omega, \tag{1}$$

where $\Delta(\cdot)$ is the Laplacian operator, $\phi(\mathbf{q})$ is the wave potential at $\mathbf{q}$, and k is the wavenumber (related directly to the wavelength, $\lambda = 2\pi/k$). The scatterer is impinged by an incident plane wave,

$$\phi^{\mathrm{I}}(\mathbf{q}) = A^{\mathrm{I}} \exp(ik\mathbf{d}^{\mathrm{I}} \cdot \mathbf{q}), \quad |\mathbf{d}^{\mathrm{I}}| = 1, \tag{2}$$

where $A^{\mathrm{I}} \in \mathbb{C}$ is the amplitude of the wave and the unit-vector $\mathbf{d}^{\mathrm{I}}$ is its direction of propagation.

Combining the Helmholtz equation and Green's second identity yields the boundary integral equation

$$c(\mathbf{p})\phi(\mathbf{p}) = \int_\Gamma \left[\frac{\partial\phi(\mathbf{q})}{\partial n} G(\mathbf{p},\mathbf{q}) - \phi(\mathbf{q}) \frac{\partial G(\mathbf{p},\mathbf{q})}{\partial n} \right] \mathrm{d}\Gamma(\mathbf{q}) + \phi^{\mathrm{I}}(\mathbf{p}), \quad \mathbf{p},\mathbf{q} \in \Gamma, \tag{3}$$

where n is the outward-pointing normal at the integration point $\mathbf{q}$ and, assuming Γ is smooth, $c(\mathbf{p}) = 1/2$. Futhermore, $G(\mathbf{p},\mathbf{q})$ is a fundamental solution to (1), representing the field effect at $\mathbf{q}$ caused by a unit-source at $\mathbf{p}$. For three-dimensional problems

$$G(\mathbf{p},\mathbf{q}) = \frac{\exp(ikr)}{4\pi r}, \tag{4}$$

where $r = |\mathbf{q} - \mathbf{p}|$.

A solution to (1) is sought subject to some boundary condition. For compact presentation, here only one boundary condition is considered:

$$\frac{\partial\phi(\mathbf{q})}{\partial n} = 0, \quad \forall \mathbf{q} \in \Gamma. \tag{5}$$

This boundary condition represents a perfectly reflecting, or "sound-hard", cylinder. Now (3) is reformulated as

$$c(\mathbf{p})\phi(\mathbf{p}) + \int_\Gamma \frac{\partial G(\mathbf{p},\mathbf{q})}{\partial n}\phi(\mathbf{q})\,\mathrm{d}\Gamma(\mathbf{q}) = \phi^{\mathrm{I}}(\mathbf{p}). \tag{6}$$

Γ is now discretised into boundary elements, such that

$$\Gamma = \bigcup_{e=1}^{E} \Gamma_e \quad \text{and} \quad \Gamma_e \bigcap \Gamma_j = \emptyset, \quad e \neq j. \tag{7}$$

Each element geometry is analytical and given by

$$\Gamma_e = \left\{\gamma_e(\xi_1,\xi_2) : \xi_1,\xi_2 \in [-1,1]\right\}, \tag{8}$$

where $\gamma_e : \mathbb{R}^2 \to \mathbb{R}^3$. For any element, the mapping between $\mathbf{q} \in \Gamma$ and (ξ_1,ξ_2) is unique and bidirectional; therefore it shall, henceforth, be assumed that any function $f(\mathbf{q})$ is equivalent to $f(\xi_1,\xi_2)$. In a conventional, polynomial BEM, the variation of potential on element e is formally expressed in a piecewise polynomial basis

$$\phi^e(\mathbf{q}) = \sum_{j=1}^{J} N_j(\xi_1,\xi_2)\phi_j^e, \tag{9}$$

where J is the number of nodes on the element; N_j and ϕ_j^e are the shape function and unknown potential, respectively, for node j.

Eq. (9) represents a conventional approach. Partition-of-unity introduces a linear expansion of plane waves on each shape function such that (9) is rewritten

$$\phi^e(\mathbf{q}) = \sum_{j=1}^{J} N_j(\xi_1,\xi_2) \sum_{m=1}^{M} A_{jm}^e \exp(ik\,\mathbf{d}_{jm}^e \cdot \mathbf{q}), \quad |\mathbf{d}_{jm}^e| = 1, \tag{10}$$

where M is the number of plane waves in the expansion at each node, $\mathbf{d}_{jm}^e \in \mathbb{R}^3$ are the prescribed plane wave directions in the basis and $A_{jm}^e \in \mathbb{C}$ are their unknown amplitudes.

The substitution of (10) into (6) gives

$$\frac{1}{2}\phi(\mathbf{p}) + \sum_{e=1}^{E}\sum_{j=1}^{J}\sum_{m=1}^{M}\int_{-1}^{1}\int_{-1}^{1} \frac{\partial G(\mathbf{p},\mathbf{q})}{\partial n} N_j(\xi_1,\xi_2)\exp(ik\,\mathbf{d}_{jm}^e\cdot\mathbf{q})|J_{\mathbf{q}}|\,\mathrm{d}\xi_1\mathrm{d}\xi_2\,A_{jm}^e = \phi^{\mathrm{I}}(\mathbf{p}), \tag{11}$$

where $|J_{\mathbf{q}}|$ is the Jacobian of the mapping in (8). While $\partial G/\partial r$ is a singular function, $\partial r/\partial n$ regularises it. Therefore, the integrals in (11) contain no singularities and can be evaluated using standard quadrature.

To find the potential on Γ, (11) is collocated at a sufficient number of points on Γ to yield a system of linear equations,

$$[(1/2)\mathbf{C} + \mathbf{H}]\{\mathbf{x}\} = \{\mathbf{b}\}, \tag{12}$$

where the sparse, square matrix $\mathbf{C}$ results from interpolations of the plane waves through (10) and the square matrix $\mathbf{H}$ is fully populated with the boundary integrals from (11). The right-hand side vector $\{\mathbf{b}\}$ contains the incident wave potentials, at the collocation points, defined in (2), and the unknown vector $\{\mathbf{x}\}$ contains the amplitudes, A^e_{jm}. Eq. (12) can be solved in a conventional fashion using an appropriate scheme.

The choice of M is dependent on the wavenumber k of the problem. As k increases (and λ decreases), the total number of degrees of freedom (N_{dof}) required to obtain a solution of a certain accuracy increases. The variable τ is introduced, defined as N_{dof} divded by the number of wavelengths in the problem; for the unit-radius sphere, this is

$$\tau = \sqrt{\frac{\pi N_{\text{dof}}}{k^2}}. \tag{13}$$

For conventional BEM simulations (without partition-of-unity enrichment), $\tau \approx 10$ is required for simulations with a 1% error. For PU-BEM simulations, only $\tau \approx 3$ is required for low wavenumbers; for higher k, τ can be reduced towards 2 [26].

3. Generating uniform points on a sphere

3.1. Discretised cube boundary method

While in two dimensions, the uniform spacing of directions around the unit circle is a trivial problem, the move to three dimensions presents a greater difficulty, since it is not generally possible, and certainly not intuitive, to define a uniform division of the 4π solid angle. There are also some trivial cases relating to the vertices and/or faces of the platonic solids. But in order to take full advantage of the plane wave basis methods in wave modelling, considerably larger numbers of directions are desirable.

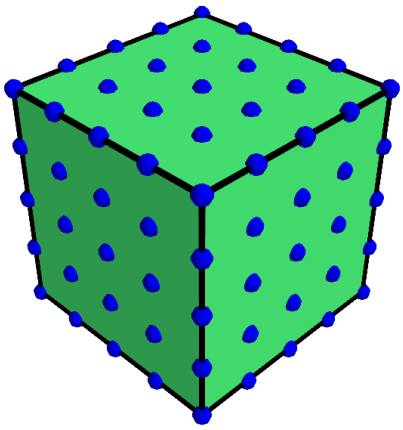

Figure 1: Uniform boundary meshing of a cube

A simple method has been used by the authors in their work to date, and this involves a uniform boundary meshing of a cube, such as the 5×5 case shown in Figure 1. A reasonably well spaced set of directions is defined by the vectors joining the centre of the cube to each 'node' on the cubes boundary. For the application in question, the accuracy of wave propagation solutions does not seem to be sensitive to the moderately small non-uniformity of spacing, and so this approach has been satisfactory. However, the method is limited to a few special cases of M for which a boundary-meshed cube is available, specifically $M = 6p^2 + 2$ (where $p \in \mathbb{Z}^+$), allowing $M = 8, 26, 56, 98, \ldots$. This imposes a significant limitation on the computational efficiency since, if one considers the variable τ defined in (13), it is likely that one requires a value that lies in between those contained in this set to optimise performance.

The new method described herein overcomes this limitation and, moreover, provides a greater uniformity of spacing compared to the discretised cube boundary method.

3.2. Coulomb force method

Consider a sphere of unit radius and of surface S on which lie particles at locations described by vectors $\mathbf{u}_i$, $i = 1, 2, \ldots, M$. Let these particles each have unit mass and unit electrical charge so that they repel each other with Coulomb forces varying with $1/|\mathbf{r}|^2$ where $r = \mathbf{u}_i - \mathbf{u}_j$. In a suitably damped system, the particles will find a static equilibrium state in which they occupy

quasi-uniform spacing. We use a simple explicit time-stepping scheme, but require no stiffness term since the particles are free to float on S.

Starting from a random set of vectors $\mathbf{u}_i^0$, the superscript denoting the time at which a quantity acts, the Coulomb force vector $\mathbf{F}_i$ at time t is given by

$$\mathbf{F}_i^t = A \sum_{j=1}^{n} \frac{(1-\delta_{ij}) \times \mathbf{r}}{|\mathbf{r}|^3}, \tag{14}$$

where A is a scalar multiplier and δ_{ij} is the Kronecker delta. This will be oriented away from S, and so we define vector $\mathbf{f}_i$ as the projection of $\mathbf{F}_i$ on S which, since the $\mathbf{u}_i$ are unit vectors, is given by

$$\mathbf{f}_i^t = (\mathbf{F}_i^t \times \mathbf{u}_i^t) \times \mathbf{u}_i^t. \tag{15}$$

The acceleration, $\ddot{\mathbf{u}}_i$, of each particle is

$$\ddot{\mathbf{u}}_i^t = \mathbf{f}_i^t - c\dot{\mathbf{u}}_i^t, \tag{16}$$

where c is an equivalent viscous damping coefficient and $\dot{\mathbf{u}}_i$ is the velocity of the particle. The velocity and position at the subsequent time, $t + \Delta t$, are given by

$$\dot{\mathbf{u}}_i^{t+\Delta t} = \dot{\mathbf{u}}_i^t + \ddot{\mathbf{u}}_i^t \Delta t, \tag{17}$$

$$\hat{\mathbf{u}}_i^{t+\Delta t} = \mathbf{u}_i^t + \dot{\mathbf{u}}_i^t \Delta t, \tag{18}$$

$$\mathbf{u}_i^{t+\Delta t} = \frac{\hat{\mathbf{u}}_i^{t+\Delta t}}{\left|\hat{\mathbf{u}}_i^{t+\Delta t}\right|}, \tag{19}$$

where (19) is used to normalise the position vectors to relocate the particles back onto S. Equations (14) to (19) are repeated in a time-stepping scheme to convergence.

An appropriate measure of the performance of the method is the minimum angle, ρ, between any two vectors $\mathbf{u}_i$ and $\mathbf{u}_j$, i.e.

$$\rho = \min \left(\cos^{-1} \frac{\mathbf{u}_i \cdot \mathbf{u}_j}{|\mathbf{u}_i||\mathbf{u}_j|} \right) \quad i = 1, \ldots, M;\ j = 1, \ldots, M;\ i \neq j. \tag{20}$$

An effective method will maximise ρ for an arbitrary M.

A study of repeated runs having the same M shows that the converged values of $\mathbf{u}_i$ are different for each run. This is expected because of the random initial $\mathbf{u}_i^0$ and the freely floating nature of the particles. However, they differ

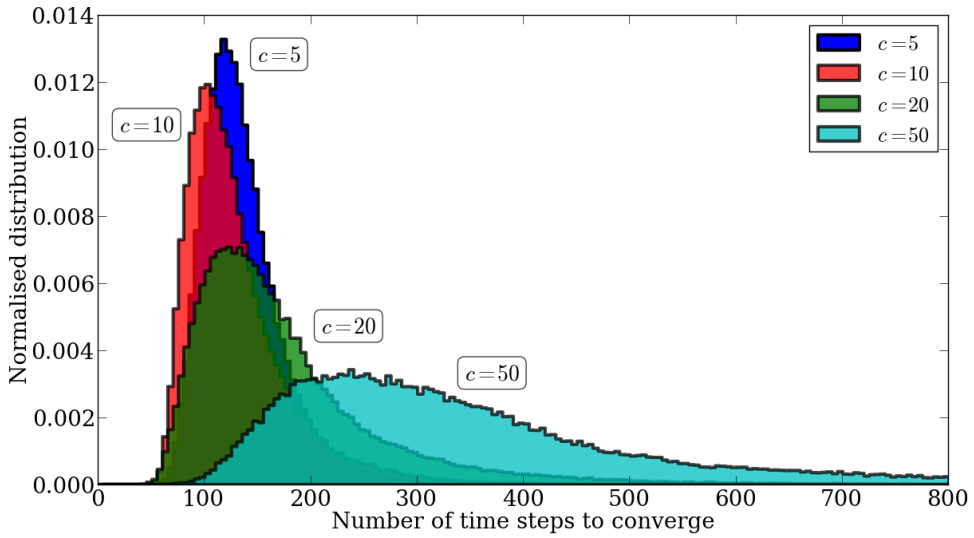

Figure 2: Histogram showing distributions of number of iterations required to converge to $0.99\rho_M$ for $M = 50$

only in the local coordinate system in which the system is viewed; i.e. the values of ρ are the same for the same M.

It remains to determine suitable values of the parameters A, c and Δt. If the damping c is too low, the particles may exhibit large oscillatory behaviour and require more time steps to reach an equilibrium position, if they indeed converge at all. Similarly, if c is too high, a large number of times steps (or a large scalar A) will be required to reach an equilibrium position.

Numerical tests show $A = 100$ and $\Delta t = 0.01$ provide for convergence for $M < 100$. The determination of a suitable damping c may be found by considering the statistical distribution of the number of iterations required to reach 99% of the converged minimum angle ρ_M. As an illustrative example, Figure 2 shows distributions of convergence rates for the case of $M = 50$ for four values of damping: $c = 5, 10, 20, 50$. Similar figures can be produced for other values of M.

Distributions such as those in Figure 2 can be approximated by log-normal distributions. For damping values $c = 1, 5, 10, 15$ and a range of M, suitably-sized samples were obtained from which the mean, μ, and variance, σ, of each distribution's natural logarithm were calculated using the maximum likelihood method. The values of μ are shown in Figure 3. From this figure,

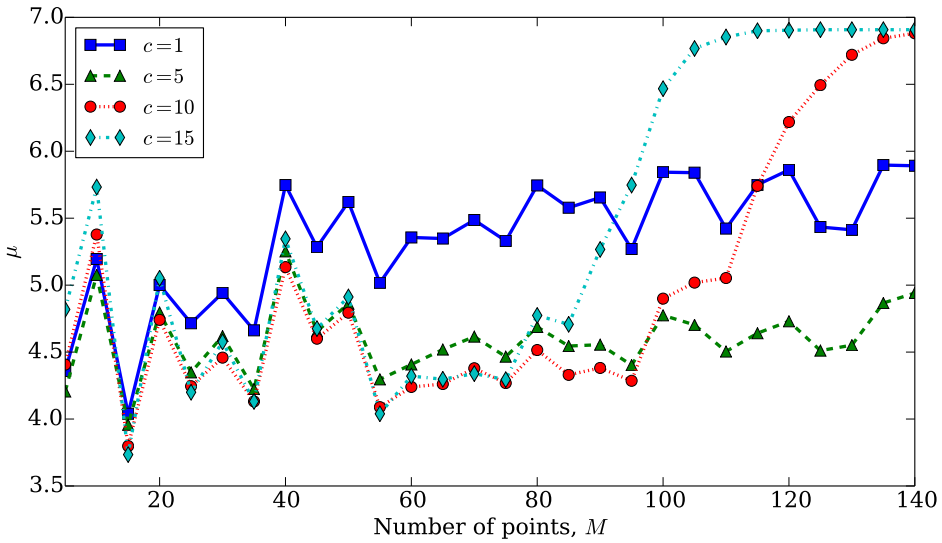

Figure 3: Natural logarithm means, μ, of distributions similar to Figure 2 (Sample sizes: 1000)

it is clear that $c = 1$ requires, on average, more time steps to converge to a $0.99\rho_M$ solution than higher values of c; this is due to the large oscillations of the particles with low damping. The distributions at higher values of c have similar means, μ, at low values of M. However, simulations with damping values $c = 10$ and $c = 15$ both become slow to converge as M increases towards 140; indeed, none of the calculations with $c = 15$ for $M > 120$ converged within 1000 time steps.

Figure 3 only gives an idea of the mean number of time steps required to obtain a $0.99\rho_M$ solution. A low variance is also desirable. Individual values of σ are not simple to interpret. Instead, the cumulative distribution function can be used to predict the likelihood that a simulation will have converged to a $0.99\rho_M$ solution in a given number of time steps. Figures 4 and 5 show this likelihood for 300 and 500 time steps respectively. For simulations of $M < 80$, 300 time steps and a damping value of $c = 5$ converge in the vast majority of cases; the minimum likelihood of converging to a $0.99\rho_M$ solution is 99.1% ($M = 5$). The other values of damping considered here provide a less certain performance. For simulations of $M \geq 80$, a damping value of $c = 5$ is also suitable but 500 time steps are recommended; the minimum likelihood of a $0.99\rho_M$ solution drops to 93.6% ($M = 140$). It should be

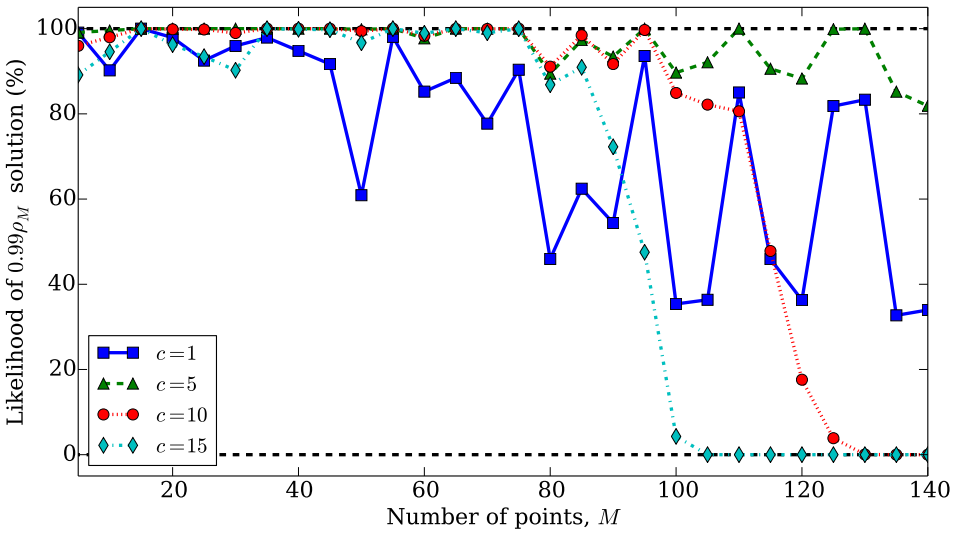

Figure 4: Likelihood of $0.99\rho_M$ solution within 300 time steps, calculated using the cumulative distribution function

noted that the solutions outside $0.99\rho_M$ still exhibit a greater ρ than the discretised cube boundary method.

From the analysis above, the authors adopt $c = 5$ with $A = 100$ and $\Delta t = 0.01$; they use 300 time steps for simulations of $M < 80$ and 500 time steps for simualtions of $80 \leq M \leq 140$. For $M > 140$, the method exhibits instability using the above parameters and a reduced time step of 0.001 is recommended.

In some applications it may be desirable to bias the directions in one direction or another. In the partition-of-unity finite element formulation for wave diffraction analysis, for example, there may be knowledge of the dominant wave direction. This may come from our physical understanding of the nature of the problem, e.g. scattered waves becoming radial at a large distance from the scatterer, or as the product of some adaptive strategy.

Such a biasing can be achieved by including an external point charge at a desired location. This should have a negative charge such that it attracts the particles on the surface of the sphere (methods using a positive repulsive charge diametrically opposite to the desired concentration do not produce as good a clustering). The point charge needs to be placed off the sphere so that it produces the desired effect without danger of producing very large

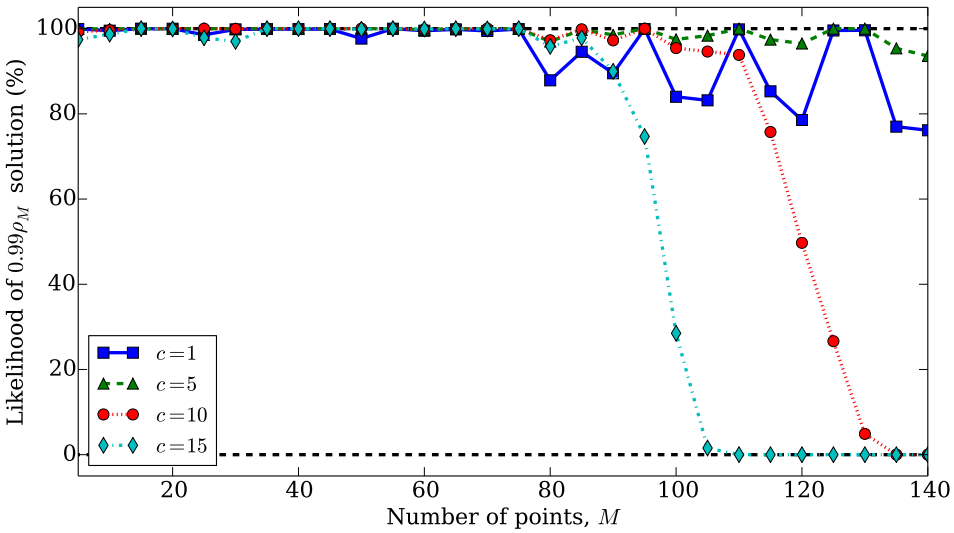

Figure 5: Likelihood of $0.99\rho_M$ solution within 500 time steps, calculated using the cumulative distribution function

attractive forces should one of the particles become almost coincident with the external charge. Typically a charge of approximately half the combined charges of the other particles, and located at a radius of 1.5, produces a reasonable concentration, though this value can be varied as required to achieve any arbitrary degree of clustering.

It is found that the introduction of an external charge greatly reduces the robustness of the method and the equilibrium can be difficult to achieve, particularly for high M. In order to counteract this instability, it is recommended that the reduced time step of 0.001 be adopted for all M if trying to obtain a set of biased points.

4. Example solutions

Figure 6a shows a solution for the case $M = 8$ as determined by the discretised cube boundary method; lines have been added to help show how these are the vertices of a cube. Figure 6b shows the same case but determined by the Coulomb force method; the lines added show that this appears like two faces of a cube that are rotated 45° from each other.

This is an interesting case as both methods produce an equally spaced

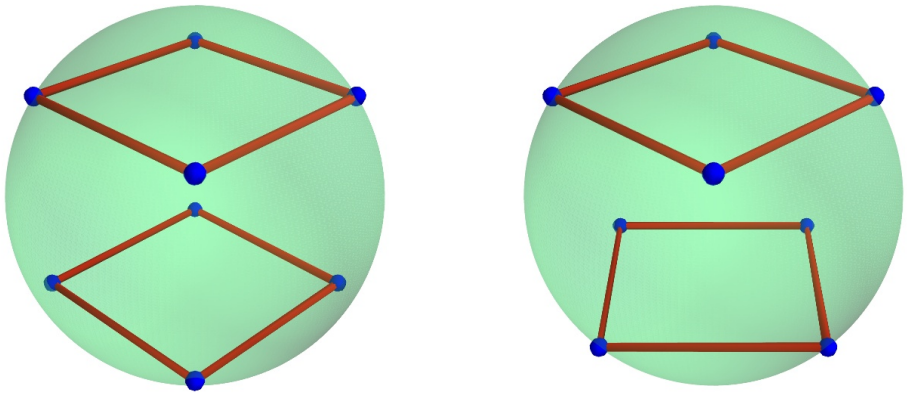

(a) Discretised cube boundary solution (b) Coulomb force solution

Figure 6: Converged solutions, $M = 8$

distribution of points with an equal minimum distance between points – approximately $2/\sqrt{3}$. However, the equilibrium states exhibit slightly different values of ρ. For the discretised cube boundary, the minimum angle between points is $\rho = 70.5°$; this is lower than that for Coulomb force solution which exhibits $\rho = 71.7°$.

If the solution of the discretised cube method is used as the initial vectors for the Coulomb force method, the system will converge immediately to that configuration ($\rho = 70.5°$). For any other initial vectors, the system will converge to $\rho = 71.7°$. The authors conclude that the latter solution is a lower potential energy state to which random systems will converge. This is made possibly more interesting when one considers that the discretised cube method solution corresponds to the vertices of a platonic solid – the cube in this case. Intuition might suggest that the vertices of such solids correspond with low energy states; this is a counterexample to this hypothesis.

The improvement in ρ is found consistently for the different M that can be obtained by the discretised cube boundary method. These are summarised in Table 1.

Figure 7 shows the solution for the case $M = 152$ determined by both methods. The points in Figure 7a appear to be uniformly spaced in portions of the sphere; however, it is clearly more densely populated with points towards the top-right of the sphere than the bottom. Conversely, the points

p	M	ρ (cube)	ρ (Coulomb)
1	8	70.5°	71.7°
2	26	35.3°	38.8°
3	56	22.0°	26.7°
4	98	15.8°	20.7°
5	152	12.3°	16.3°

Table 1: Comparison of values of ρ from discretised cube boundary solutions and converged Coulomb force solutions

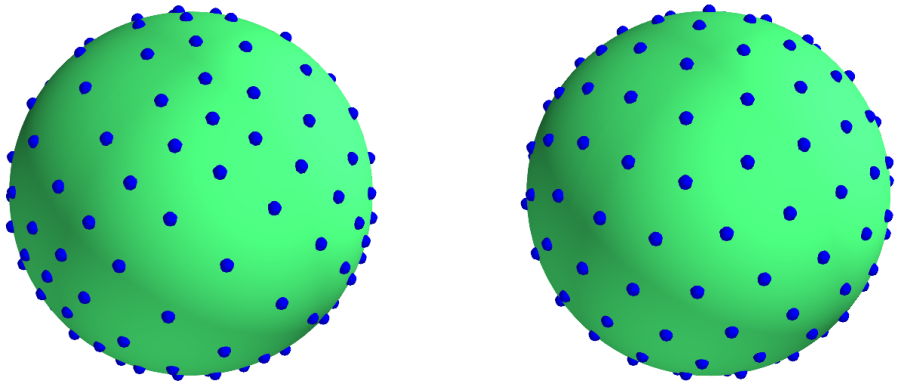

(a) Discretised cube boundary solution (b) Coulomb force solution

Figure 7: Converged solutions, $M = 152$

Figure 7b appear to be uniformly spaced over the entire sphere.

Figure 8 displays the same solutions as Figure 7 but projected on a planar azimuth-inclination space. Despite the distortion from projecting a sphere onto a square graph, the differences are clear. Considering a central latitudinal strip, Figure 8a shows clear irregularities in the spacing of points while Figure 8b shows a more uniform spacing.

Finally, Figure 9 shows the converged solution for a case in which clustering of particles is required. Arbitrarily, the case of $M = 71$ is considered, with an external charge located at a radius of 1.5. The points are clearly clustered towards one point on the sphere. This point can be prescribed by fixing the position of the external charge.

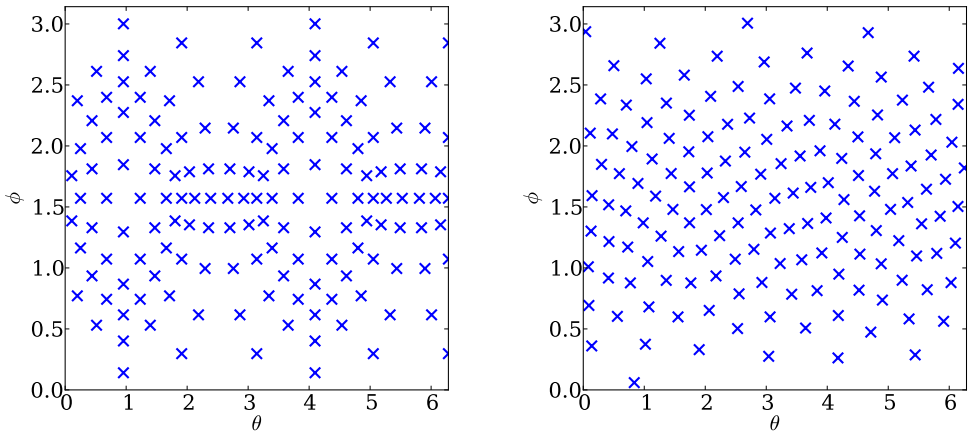

(a) Discretised cube boundary solution (b) Coulomb force solution

Figure 8: $M = 152$ solutions, represented using spherical coordinates of points: θ azimuth, ϕ inclination

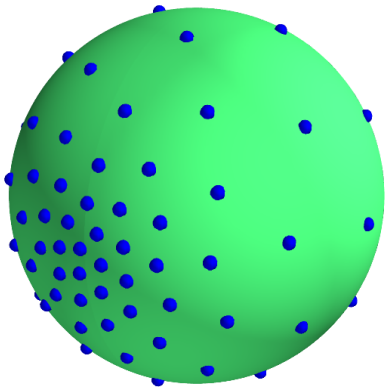

Figure 9: Particle clustering, $M = 71$

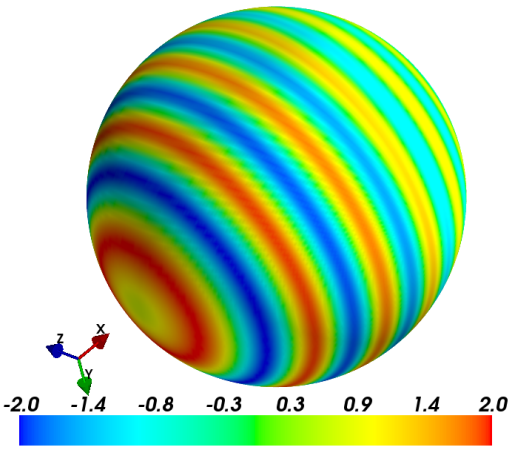

Figure 10: Scattering by a sphere at $k = 20$. Isovalues of the real-part of acoustic potential are shown.

5. Numerical results

The following numerical results are from simulations of a plane wave impinging a unit-radius, perfectly scattering sphere. Assuming the incident wave is propagating in the direction $\mathbf{d}^{\mathrm{I}} = [1, 0, 0]$, the scattered acoustic potential at any point $\mathbf{x}(r, \theta)$ can be found with the analytical solution [27]:

$$\phi_{\mathrm{S}}(r, \theta) = \sum_{n=0}^{\infty} -\frac{i^n (2n+1) j_n'(ka)}{h_n'(ka)} P_n(\cos\theta) h_n(kr) \tag{21}$$

where j_n is the spherical Bessel function of the first kind, h_n is the spherical Hankel function of the first kind, P_n is the Legendre function of the first kind and a is the radius of the sphere; in these examples, $a = 1$. A visual representation of the real part of the potential over the surface of the sphere can be seen in Figure 10.

The authors use a collocation PU-BEM employing the CHIEF method [28] to overcome any nonuniqueness in the formulation. In order to remove any integration error, matrix entries are calculated using a 50×50 Gauss quadrature with each element subdivided into integration cells with sides no longer than $\lambda/4$. The linear system of equations is solved using singular value

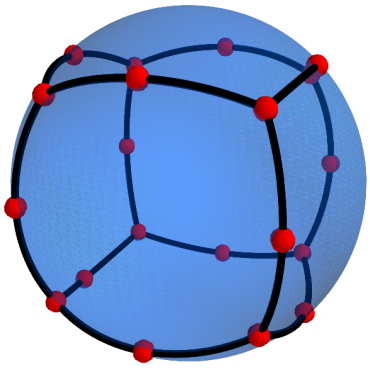

Figure 11: Representation of the sphere mesh: black lines represent element edges; small red spheres represent nodal points.

decomposition (SVD). Errors, $\mathcal{E}$, are evaluated in a relative L^2-norm sense,

$$\mathcal{E} = \frac{\left\| \mathbf{\Phi} - \mathbf{\Phi}^{\text{exact}} \right\|_{L^2(\Gamma)}}{\left\| \mathbf{\Phi}^{\text{exact}} \right\|_{L^2(\Gamma)}}, \tag{22}$$

where $\mathbf{\Phi}$ is a vector containing complex potentials at points on the sphere obtained using the PU-BEM simulation; $\mathbf{\Phi}^{\text{exact}}$ is a vector of complex potentials calculated using (21).

The sphere is discretised into 6 quadratical, 8-noded elements. Analytical geometry points can be obtained by using a cube-to-sphere mapping: consider a cube with coordinates $\bar{x}, \bar{y}, \bar{z} \in [-1, 1]$; any point $(\bar{x}, \bar{y}, \bar{z})$ on the surface on the cube can be mapped to a point (x, y, z) on the surface of the unit-radius sphere with the mapping

$$\begin{aligned} x &= \bar{x}\sqrt{1 - \frac{\bar{y}^2}{2} - \frac{\bar{z}^2}{2} + \frac{\bar{y}^2\bar{z}^2}{3}}, \\ y &= \bar{y}\sqrt{1 - \frac{\bar{x}^2}{2} - \frac{\bar{z}^2}{2} + \frac{\bar{x}^2\bar{z}^2}{3}}, \\ z &= \bar{z}\sqrt{1 - \frac{\bar{x}^2}{2} - \frac{\bar{y}^2}{2} + \frac{\bar{x}^2\bar{y}^2}{3}}. \end{aligned} \tag{23}$$

The meshed sphere can be seen in Figure 11.

In order to make direct comparisons between the new Coulomb force method and the discretised cube boundary method of choosing plane wave

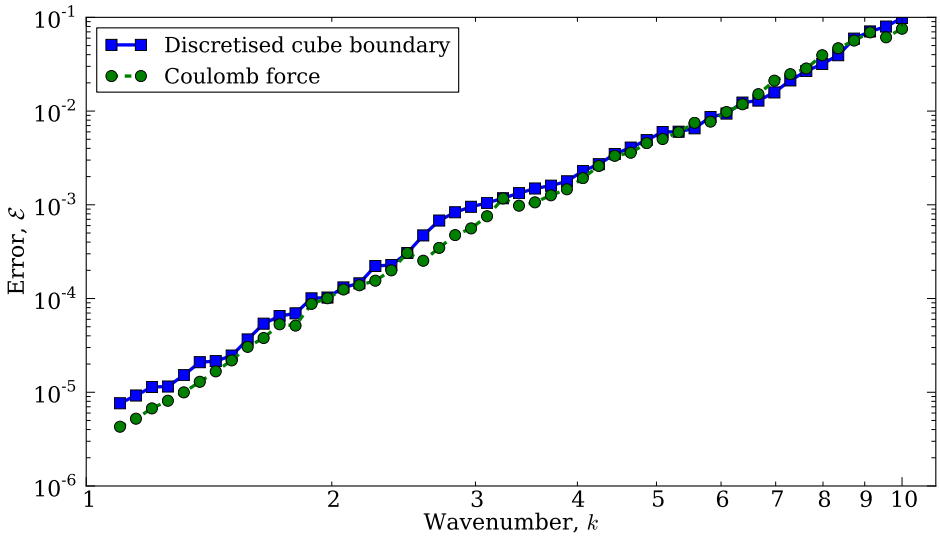

Figure 12: Comparison of accuracy of PU-BEM simulations using different methods to choose $M = 8$ wave direction in the enrichment.

directions, the case of $M = 8$ is considered. The inclusion of the incident plane wave direction in the partition-of-unity expansion has been found beneficial in two dimensions [29]. The authors also found it improved the accuracy of simluations in three dimensions. To include this wave direction with the Coulomb force method, one charge can be fixed in the time stepping scheme (as described in the previous section). With the discretised cube boundary method, a rotation must be applied to the solution unless a point is already coincident with the incident plane wave direction.

Figure 12 shows the errors, $\mathcal{E}$, of PU-BEM simulations using these methods. Though the results at some wavenumbers appear to favour the Coulomb force method, the results show no clear distinction in accuracy between the two. As the total number of degrees of freedom, N_{dof}, used in all the simulations is 80, the value of τ decreases as k increases; this causes the errors of the simulations to increase gradually as k increases. In order to achieve more accurate simulations, refinement by either increasing the number of elements/nodes and/or planewaves in the expansion is required.

Figure 13 shows the condition numbers of the BEM system matrices of each simulation. The conditioning of the system matrix improves as the value of τ decreases. Figure 13 does not show a significant difference between the

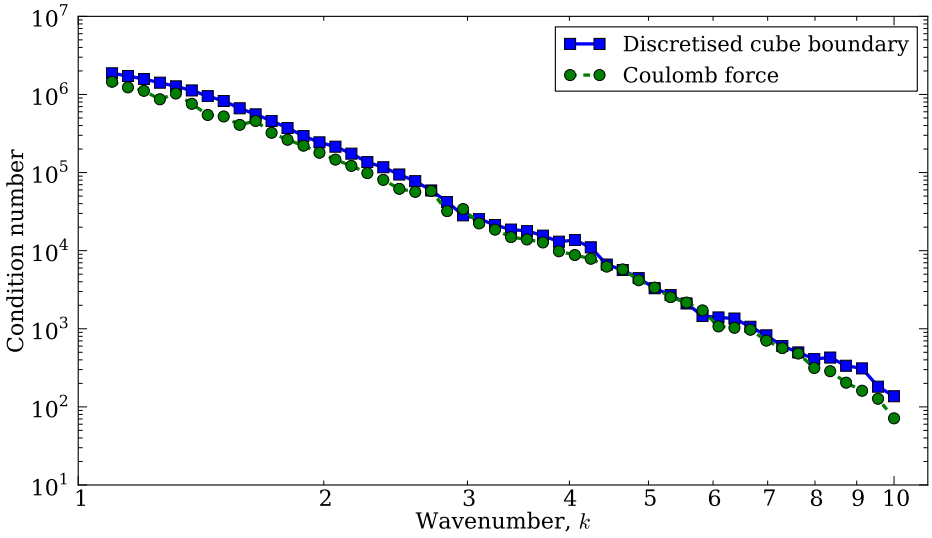

Figure 13: Comparison of condition numbers of PU-BEM simulations using different methods to choose $M = 8$ wave directions in the enrichment.

discretised cube boundary and Coulomb force methods.

While the previous example shows that the Coulomb force method does not improve the accuracy of PU-BEM simulations given a value of M that can be obtained with discretised cube boundary method, the principal advantage of the new method is in the ability to choose an arbitrary M. For example, if it is established, from (13), that $M = 30$ would provide a prescribed error, using the discretised cube boundary method to choose wave directions of the PU-BEM enrichments results in running a simulation with $M = 56$ (the lowest available). The computational operations required for PU-BEM system matrices are of $\mathcal{O}({N_{\text{dof}}}^2)$ for building and $\mathcal{O}({N_{\text{dof}}}^3)$ for solving. This would increase the total number of operations (and therefore time for simulation) significantly for each enriched node using the higher M. As the number of elements in the mesh increases, so does the computational expense of using the extra plane waves. It is, therefore, extremely desirable to have the flexibility which is offered by the new approach to choose the exact number of plane waves desired.

Figure 14 displays the N_{dof} required in order to obtain an error of "engineering precision", which the authors define as $\mathcal{E} \sim 1\%$. The figure shows the large discrete increases in M – and therefore N_{dof} – required when using

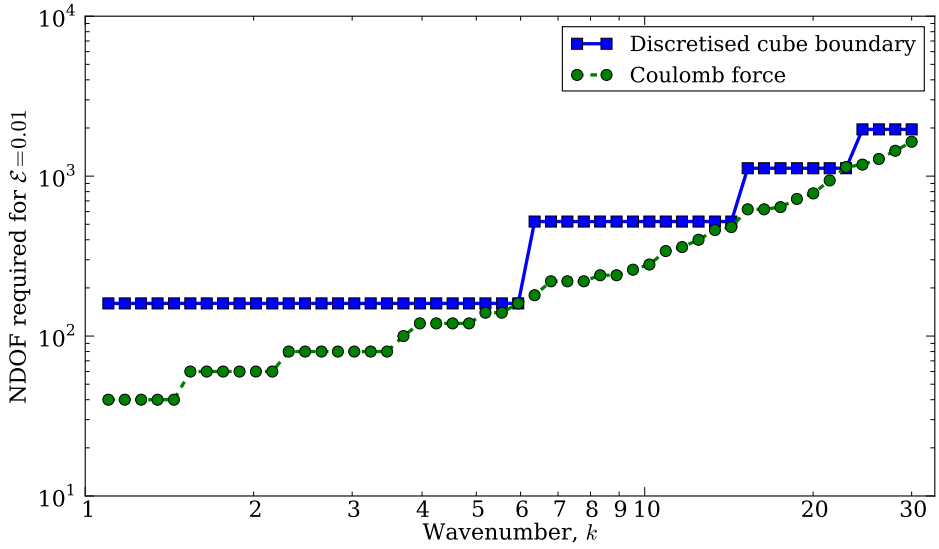

Figure 14: Comparison of number of degrees of freedom required to obtain 1% error with PU-BEM simulations using different methods to choose wave directions in the enrichment.

the discretised cube boundary method. In comparison, much smaller discrete increases in NDOF are required when using the Coulomb force method. The curves interpolate at the few coincidential points where the M required to obtain a 1% error is equal to a value that can obtained using the discretised cube boundary method.

Figure 15 shows the value of τ of each simulation in Figure 14. Two trends are noted. First, there is a significant rise in τ when M (and therefore N_{dof}) rises using the discretised cube boundary method. At low wavenumbers, this leads to values of $\tau > 10$ which is higher than that required for an error $\mathcal{E} \sim 1\%$ using the conventional BEM. This also has a negative impact on the conditioning of the PU-BEM system matrix which becomes susceptible to errors in the solution so requires a more robust solver. Secondly, the overall trend is that the τ required to obtain an error $\mathcal{E} \sim 1\%$ falls as k increases. For $k = 30$, a value $\tau \approx 2.4$ (1640 degrees of freedom) was required for the PU-BEM simulation using the Coulomb force method; in comparison, a conventional BEM simulation with $\tau \approx 10$ would require approximately 28,640 degrees of freedom.

Figure 16 is similar to Figure 14 but shows the N_{dof} required but for

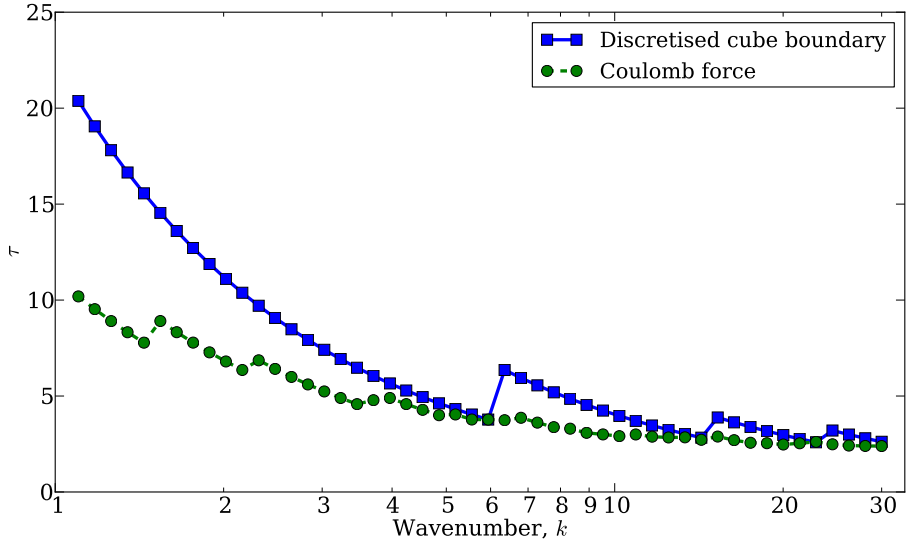

Figure 15: Comparison of τ required to obtain 1% error with PU-BEM simulations using different methods to choose wave directions in the enrichment.

a smaller error: $\mathcal{E} \sim 0.1\%$. The same pattern as Figure 14 is observed, demonstrating the principal advantage of the Coulomb force method: the ability to choose an arbitrary M.

As discussed above, the N_{dof} of a simulation has a direct impact on the runtime, due to the operations required to build and solve the PU-BEM system. It should be noted that in a direct comparison of runtimes between the Coulomb force method and discretised cube method, the former takes significantly longer due to the time-stepping nature of the scheme. Despite this, the process of finding plane wave directions still constitutes less than 0.1% of the total runtime of all the PU-BEM simulations in this work (for $M < 100$, the Coulomb force method runtime was < 1 second). Figure 17 plots the normalised total runtimes of the simulations in Figure 16. With similar steps steps in the curves, the two figures show a strong correlation; Figure 17 demonstrates that the extra runtime required to use the Coulomb force method is insignificant over the period of the entire simulation.

6. Conclusions

This paper has presented a new method for producing evenly spaced distributions of arbitrary numbers of points on a spherical surface. Although

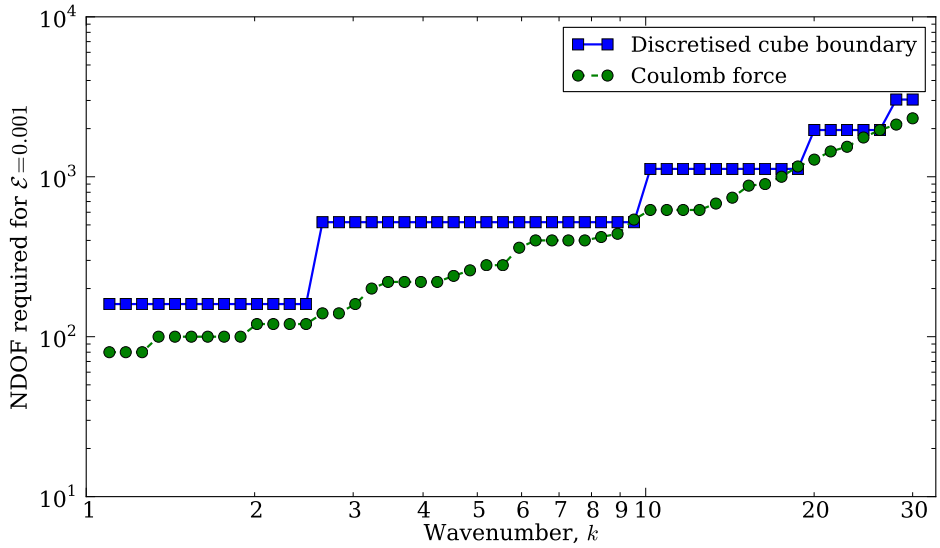

Figure 16: Comparison of number of degrees of freedom required to obtain 0.1% error with PU-BEM simulations using different methods to choose wave directions in the enrichment.

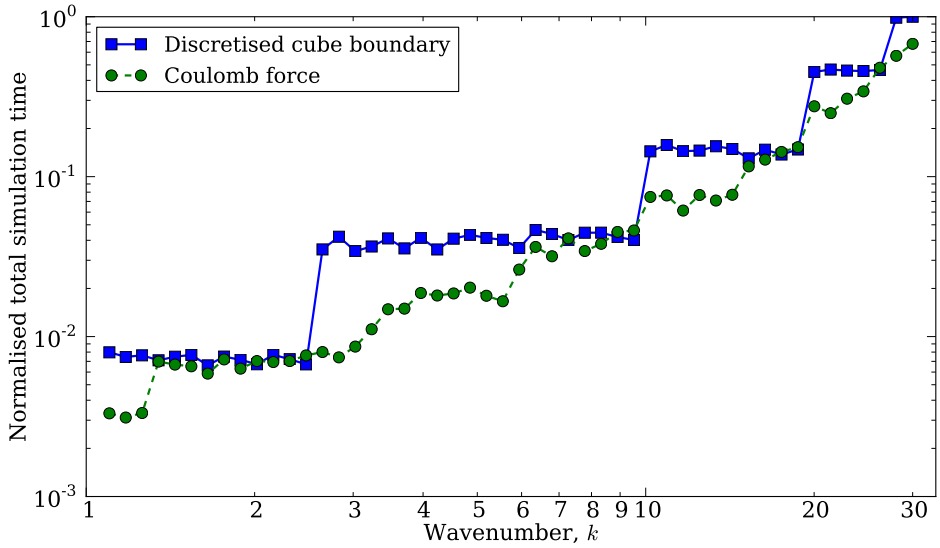

Figure 17: Comparison total simulation runtime required to obtain 0.1% error with PU-BEM simulations using different methods to choose wave directions in the enrichment.

this has widespread application in science and engineering, the motivation is the efficient solution of partition-of-unity finite and boundary element problems in 3D wave scattering.

The method is a simple one, based on the use of an explicit time stepping scheme to converge to a static equilibrium state for a set of charged particles on a spherical surface. Extensions to other geometries are straightforward. Recommendations are made for values of key parameters such as time step and damping.

The method repeatably and accurately reproduces well-known equilibrium states analogous to the platonic solids, and gives improved distributions in comparison with a discretised cube boundary method. The greatest advantage over this latter method, though, lies in the fact that arbitrary numbers of points may be evenly spaced.

The method has been extended by introducing an external charge to give rise to clustering of the directions towards a desired orientation.

Finally, numerical results of PU-BEM wave scattering simulations have been given. These results demonstrate the advantage and flexibility of choosing an arbitrary number of plane waves in a partition-of-unity expansion.

References

[1] Melenk JM, Babuška I. The partition of unity finite element method: Basic theory and applications. Computer Methods in Applied Mechanics and Engineering 1996;139(1-4):289–314. doi:10.1016/S0045-7825(96)01087-0.

[2] Perrey-Debain E, Laghrouche O, Bettess P, Trevelyan J. Plane-wave basis finite elements and boundary elements for three-dimensional wave scattering. Philosophical Transactions of the Royal Society of London Series A: Mathematical, Physical & Engineering Sciences 2004;362(1816):561–77. doi:10.1098/rsta.2003.1335.

[3] Massimi P, Tezaur R, Farhat C. A discontinuous enrichment method for three-dimensional multiscale harmonic wave propagation problems in multi-fluid and fluid-solid media. International Journal for Numerical Methods in Engineering 2008;76(3):400–25. doi:10.1002/nme.2334.

[4] Kovalevsky L, Ladevèze P, Riou H, Bonnet M. The variational theory of complex rays for three-dimensional Helmholtz prob-

lems. Journal of Computational Acoustics 2012;20(4):1250021. doi:10.1142/S0218396X1250021X.

[5] Luostari T, Huttunen T, Monk P. Error estimates for the ultra weak variational formulation in linear elasticity. ESAIM: Mathematical Modelling and Numerical Analysis 2013;47(1):183–211. doi:10.1051/m2an/2012025.

[6] Bettess P. Short-wave scattering: problems and techniques. Philosophical Transactions of the Royal Society A—Mathematical, Physical & Engineering Sciences 2004;362(1816):421–43. doi:10.1098/rsta.2003.1329.

[7] von Neumann J. Various techniques used in connection with random digits. Journal of Research of the National Bureau of Standards 1951;12:36–8.

[8] Cook JM. Rational formulae for the production of a spherically symmetric probability distribution. Mathematics of Computation 1957;11:81–2. doi:10.1090/S0025-5718-1957-0690630-7.

[9] Muller ME. A note on a method for generating points uniformly on n-dimensional spheres. Communications of the ACM 1959;2(4):19–20. doi:10.1145/377939.377946.

[10] Hicks JS, Wheeling RF. An efficient method for generating uniformly distributed points on the surface of an n-dimensional sphere. Communications of the ACM 1959;2(4):17–9. doi:10.1145/377939.377945.

[11] Sibuya M. A method for generating uniformly distributed points on n-dimensional spheres. Annals of the Institute of Statistical Mathematics 1962;14(1):81–5. doi:10.1007/BF02868626.

[12] Marsaglia G. Choosing a point from the surface of a sphere. The Annals of Mathematical Statistics 1972;43(2):645–6. doi:10.1214/aoms/1177692644.

[13] Tashiro Y. On methods for generating uniform random points on the surface of a sphere. Annals of the Institute of Statistical Mathematics 1977;29(1):295–300. doi:10.1007/BF02532791.

[14] Yang Z, Pang WK, Hou SH, Leung PK. On a combination method of VDR and patchwork for generating uniform random points on a unit sphere. Journal of Multivariate Analysis 2005;95(1):23–36. doi:10.1016/j.jmva.2004.08.012.

[15] Harman R, Vladimir L. On decompositional algorithms for uniform sampling from n-spheres and n-balls. Journal of Multivariate Analysis 2010;101(10):2297–304. doi:10.1016/j.jmva.2010.06.002.

[16] Erber T, Hockney GM. Equilibrium configurations of n equal charges on a sphere. Journal of Physics A: Mathematical and General 1991;24(23):L1369–77. doi:10.1088/0305-4470/24/23/008.

[17] Glasser L, Every AG. Energies and spacings of point charges on a sphere. Journal of Physics A: Mathematical and General 1992;25(9):2473–82. doi:10.1088/0305-4470/25/9/020.

[18] Morris JR, Deaven DM, Ho KM. Genetic-algorithm energy minimization for point charges on a sphere. Physical Review B: Condensed Matter and Materials Physics 1996;53(4):R1740–3. doi:10.1103/PhysRevB.53.R1740.

[19] Saff EB, Kuijlaars ABJ. Distributing many points on a sphere. The Mathematical Intelligencer 1997;19(1):5–11. doi:10.1007/BF03024331.

[20] Kurihara Y. Numerical integration of the primitive equations on a spherical grid. Monthly Weather Review 1965;93(7):399–415. doi:10.1175/1520-0493(1965)093¡0399:NIOTPE¿2.3.CO;2.

[21] Sahr K, White D, Kimerling AJ. Geodesic discrete global grid systems. Cartography and Geographic Information Science 2003;30(2):121–34. doi:10.1559/152304003100011090.

[22] Rubinstein RY. Generating random vectors uniformly distributed inside and on the surface of different regions. European Journal of Operational Research 1982;10(2):205–9. doi:10.1016/0377-2217(82)90161-8.

[23] Smith RL. Efficient Monte Carlo procedures for generating points uniformly distributed over bounded regions. Operations Research 1984;32(6):1296–308. doi:10.1287/opre.32.6.1296.

[24] Becker AA. The boundary element method in engineering: a complete course. Maidenhead: McGraw-Hill; 1992.

[25] Wrobel LC. The Boundary Element Method, Vol. I: Applications in Thermo-fluids and Acoustics. Chichester, UK: John Wiley & Sons, Ltd.; 2002.

[26] Perrey-Debain E, Trevelyan J, Bettess P. Plane wave interpolation in direct collocation boundary element method for radiation and wave scattering: numerical aspects and applications. Journal of Sound and Vibration 2003;261(5):839–58. doi:10.1016/S0022-460X(02)01006-4.

[27] Morse PM, Feshbach H. Methods of Theoretical Physics: Part II. McGraw-Hill; 1953.

[28] Schenck HA. Improved integral formulation for acoustic radiation problems. Journal of the Acoustical Society of America 1968;44(1):41–58. doi:10.1121/1.1911085.

[29] Peake MJ, Trevelyan J, Coates G. Extended isogeometric boundary element method (XIBEM) for two-dimensional Helmholtz problems. Computer Methods in Applied Mechanics and Engineering 2013;259:93–102. doi:10.1016/j.cma.2013.03.016.